Title
Visualizing lipid structure and raft domains in living cells with two-photon microscopy

Permalink
https://escholarship.org/uc/item/89k211z5

Journal
Proceedings of the National Academy of Sciences of the United States of America, 100(26)

ISSN
0027-8424

Authors
Gaus, Katharina
Gratton, Enrico
Kable, Eleanor PW
et al.

Publication Date
2003-12-23

DOI
10.1073/pnas.2534386100

Peer reviewed

Visualizing lipid structure and raft domains in living cells with two-photon microscopy

Katharina Gaus*†, Enrico Gratton‡, Eleanor P. W. Kable§, Allan S. Jones§, Ingrid Gelissen*, Leonard Kritharides*¶, and Wendy Jessup*

*Centre for Vascular Research at the University of New South Wales and Department of Haematology, Prince of Wales Hospital, Sydney NSW 2052, Australia; ‡Laboratory for Fluorescence Dynamics, University of Illinois at Urbana–Champaign, Urbana, IL 61801; §Australian Key Centre for Microscopy and Microanalysis, University of Sydney, Sydney NSW 2006, Australia; and ¶Department of Cardiology, Concord Hospital, University of Sydney, Sydney NSW 2139, Australia

The lateral organization of cellular membranes is formed by the clustering of specific lipids, such as cholesterol and sphingolipids, into highly condensed domains (termed lipid rafts). Hence such domains are distinct from the remaining membrane by their lipid structure (liquid-ordered vs. -disordered domains). Here, we directly visualize membrane lipid structure of living cells by using two-photon microscopy. In macrophages, liquid-ordered domains are particularly enriched on membrane protrusions (filopodia), adhesion points and cell–cell contacts and cover 10–15% of the cell surface at 37°C. By deconvoluting the images, we demonstrate the existence of phase separation *in vivo*. We compare the properties of microscopically visible domains (<1 μm^2), with those of isolated detergent-resistant membranes and provide evidence that membrane coverage by lipid rafts and their fluidity are principally governed by cholesterol content, thereby providing strong support for the lipid raft hypothesis.

membrane domains | macrophages

The lipid raft hypothesis proposes that the lateral organization of cellular membranes is based on the presence of distinct, cholesterol-rich, rigid domains (rafts) (1), which are involved in signal transduction (2), protein sorting, and membrane transport (3, 4). Our understanding of lipid structure and the formation of specific lipid domains in membranes, however, is almost exclusively based on model membrane systems (5). Although phase separation of domains of liquid-ordered structure is predicted to exist in cellular membranes (6, 7), direct demonstration using methodologies such as fluorescence quenching has been difficult to apply to living cells (8). The evidence for the existence of lipid rafts in living cells is largely based on measurements of the clustering (9, 10) or diffusion (11, 12) of lipid raft proteins, which are secondary to the lipid organization.

In the present study, we labeled living cells with the fluorescent probe 6-acyl-2-dimethylaminonapthalene (Laurdan), which has been previously used to characterize domain formation and phase separation in model membranes using phospholipid mixtures (13–15) or lipid extracted from cellular membranes (16–18). Laurdan is an environmentally sensitive fluorescence probe that exhibits a 50-nm red shift as membranes undergo phase transition from gel to fluid, due to altered water penetration into the lipid bilayer (19). Its dipole is aligned parallel to the hydrophobic lipid chains in membranes and is located in both bilayers (20). The probe's fluorescence in water is negligible, and it is not influenced spectroscopically by surface modifications such as lipoprotein binding (20, 21). The environmentally induced red shift allows the translation of intensity measurements at different wavelengths into lipid packing orders within the membranes of intact and living cells (20, 22, 23). Generalized polarization (GP), with a correcting factor G for the experimental setup, is defined analogously to fluorescence polarization by measuring the intensities (*I*) between 400 and 460 nm and 470 and 530 nm:

$$GP = \frac{I_{(400-460)} - G \times I_{(470-530)}}{I_{(400-460)} + G \times I_{(470-530)}}. \quad [1]$$

GP values range from –1 (most fluid) to +1 (most condensed) membranes and are independent of local probe concentrations. Laurdan distributes equally into fluid or condensed membranes and does not associate itself with specific fatty acids or phospholipid head groups (20); GP values therefore reflect the overall membrane structure and not a specific lipid or protein composition (22). Lipid order can be visualized by its effect on the spectroscopic properties of Laurdan, and deconvolution of the GP distribution gives additional quantitative structural information. Lipid phase boundaries for GP values were estimated by using liposomes with compositions similar to those of cellular membranes (17, 24). In liposomes with equal molar ratios of dioleoylphosphatidylcholine (DOPC), cholesterol, and sphingomyelin, GP values of >0.55 and <−0.05 represent membranes in gel and fluid phase, respectively (17). Moreover, distinct liquid-disordered/nonraft domains ($0.25 < GP < −0.05$) and liquid-ordered/raft domains ($0.55 > GP > 0.25$), which are intermediate between gel and fluid phases, are also identified in liposomes. Separation of liquid-ordered and -disordered phases at GP values between 0.2 and 0.3 has also been shown with other phospholipid mixtures (13–15).

Methods

Cells. THP-1 and RAW264.7 cells were cultured in RPMI medium 1640/10% FBS (FBS, Trace Biosciences, Castle Hill, Australia) (25). Human foreskin fibroblasts AG01518 (Coriell Cell Repositories, Camden, NJ) were cultured in DMEM (Trace Biosciences)/10% FBS. Human monocyte-derived macrophages (hMDMs) were isolated as described (26).

Tissue Culture for Microscopy. Cells were plated on coverslips at $0.1–1.2 \times 10^6$ cells per ml for 24 h (fibroblasts, RAW264.7), with 50 ng/ml phorbol 12-myristate 13-acetate (PMA) for 3 days (THP-1) or for 13 days (hMDMs). Living cells were washed, labeled with 5 μM Laurdan (Molecular Probes) for 30–60 min at 37°C, washed, mounted on an open-top microscope chamber, and sealed with hot wax. Images were recorded in phenol-red free media (+50 ng/ml PMA for THP-1). Where indicated, cells were fixed in 2% (THP-1) or 4% (RAW, fibroblasts) paraformaldehyde (Sigma) at 4°C for 20 min. For immunofluorescence, fixed cells were blocked with 5% normal donkey serum (NDS) (The Jackson Laboratory) in 0.1% saponin (Sigma) and immunolabeled for 1 h each with primary
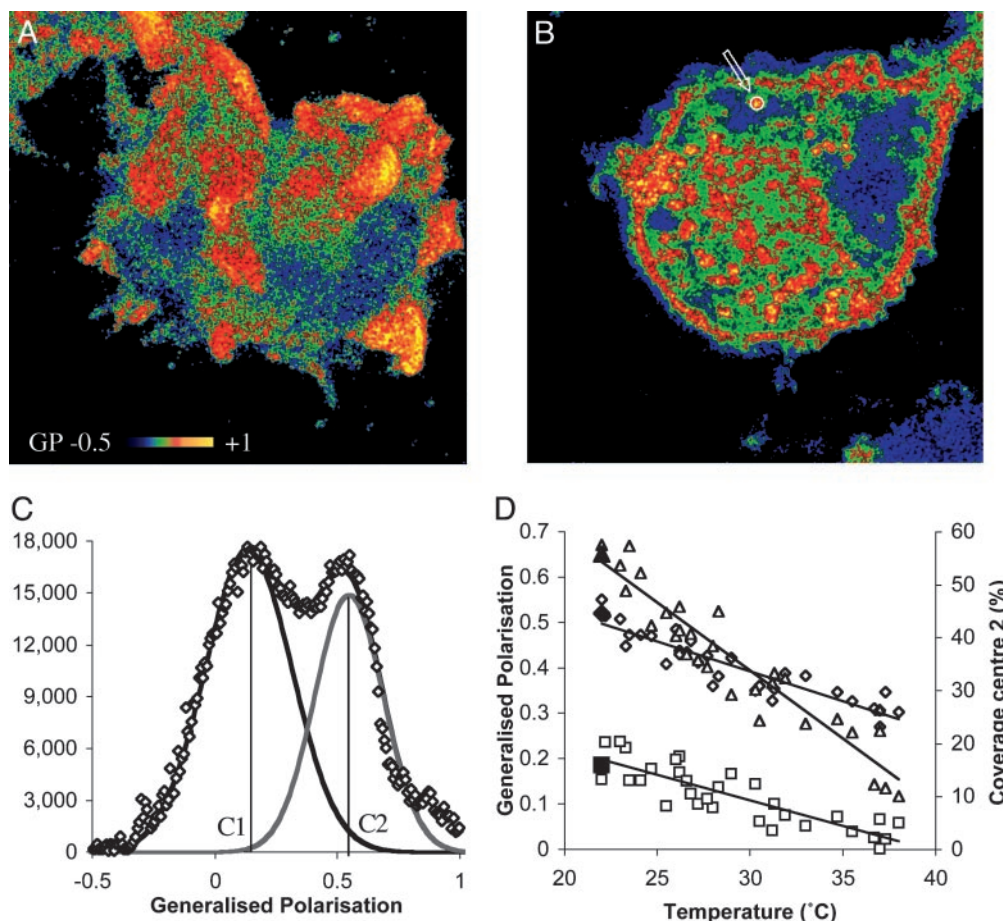
Fig. 1. GP images of living macrophages, GP distribution, and temperature dependency. 3D-reconstructed pseudocolored GP images of RAW264.7 cell (image plane parallel to coverslip, viewed from above) (*A*) and THP-1 cell (viewed from below) (*B*). Circled area (arrow) 126 pixels/0.73 μm^2; widths are 28.3 μm (*A*) and 39.0 μm (*B*). (*C*) Distribution of a stack of GP images (◇) was deconvoluted by fitting two Gaussian distributions to the experimental data (black line) with centers of GP = 0.140 (center C1) and GP = 0.549 (center C2). Area under each curve equates to surface coverage. (*D*) Temperature dependence of the GP centers (□, C1, slope −0.0112; ◇, C2 slope −0.0132; left axis) and coverage of center C2 as percent of all Laurdan-stained pixels (△ slope −3.566, right axis). Solid symbols are the means of 10–12 stacks (Table 1); open symbols are data from single stack.

rabbit anti-cavolin-1 (Santa Cruz Biotechnology); mouse anti-flotillin-1; mouse anti-caveolin-2 (both from Transduction Laboratories, Lexington, KY); mouse anti-transferrin receptor (Zymed); or rabbit anti-ABCA1 (Novus Biologicals, Littleton, CO, all diluted 1:100) and secondary antibodies Cy3-conjugated donkey anti-rabbit IgG or Cy5-conjugated donkey anti-mouse IgG (both from The Jackson Laboratory, diluted 1:200) in PBS with 5% NDS/0.1% saponin then washed and mounted with Antifade (Molecular Probes). No nonspecific binding or crossreaction between secondary mouse and rabbit antibodies was observed. Where indicated, cells were treated with 0–10 mM methyl β-cyclodextrin (mCD, Sigma) for 0–1 h at 22°C or 37°C in media with 1 mg/ml BSA (essentially fatty acid free, Sigma). Crosslinking of fibroblasts used 0.5 mM BS^3 [bis(sulfosuccinimidyl)suberate, Pierce, Dorra, Australia] at 4°C for 45 min in PBS (27). For patching of domains, living fibroblasts were treated with mouse antitransferrin receptor (1:100) in DMEM with 2 mg/ml BSA for 45 min at 10°C, washed, and incubated with donkey anti-mouse IgG (1:100) in DMEM with 2 mg/ml BSA for 45 min at 10°C (28).

Lipid raft isolation used postnuclear supernatants of whole-cell homogenate (15 × 10^6 cells) or purified plasma membranes (50 × 10^6 cells) (29). Samples were sonicated for 30 sec (whole-cell homogenate) or 120 sec (plasma membranes) with a high-power output probe sonicator or treated with detergent for

30 min on ice (0.2% Triton X-100 or 0.2% Lubrol WX) and separated on a 45–5% sucrose gradient (16 h at 198,000 × g_{av} in a swing-out rotor (SW41, Beckman Coulter) as described (30). Rafts were collected at densities of 1.060–1.090 g/ml and nonraft material at 1.150–1.180 g/ml.

Microscopy. Images were obtained with a DM IRE2 Microscope (Leica, Gladesville, Australia). Laurdan fluorescence was excited with a mode-locked titanium–sapphire laser (Verdi/Mira 900, Coherent Radiation, Palo Alto, CA). Two-photon intensity input was regulated with an amplitude modulator linked to the Leica software system. For living cells a ×63 water objective, numerical aperture (NA) = 1.2 and for fixed cells a ×100 oil objective, NA = 1.4 was used. To record intensities at selective wavelengths, internal photon multiplier tubes collected images in an eight-bit, unsigned images with 512 × 512 pixels at a 400-Hz scan speed. Laurdan intensity images were recorded simultaneously with emission in the range of 400–460 nm and 470–530 nm for the two channels, respectively. The relative sensitivity of the two channels was determined with 0.5 μM Laurdan in DMSO for each experiment and the G-factor calculated. For confocal microscopy, a helium-neon laser (green and blue) line was used to excite Cy3 [excitation (Ex): 543 nm; emission (Em): 550–620 nm] and Cy5 (Ex: 633 nm, Em 650–720 nm) with appropriate cutoff filters and minimal pinhole widths.
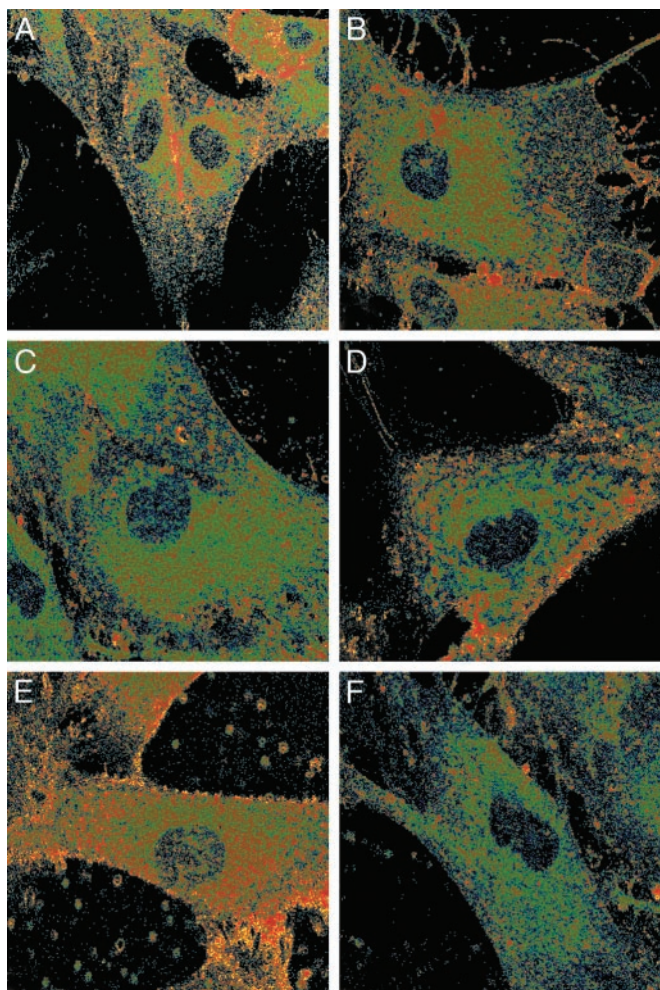
CELL BIOLOGY

Fig. 2. GP images of fibroblasts. GP image of living (*A*) or fixed (*B*) fibroblasts (4% paraformaldehyde, 30 min, 4°C) were obtained as described for macrophages. Cells were treated with 10 mM mCD for 1 h at 37°C (*C*), nonspecifically crosslinked with 0.5 mM BS[3] (*D*), or patched with anti-transferrin receptor and secondary antibodies (*E*). For *F*, fibroblasts were first mCD-treated and then antibody patched. The same pseudocoloring as in Fig. 1 was used. The widths of the images are 114.0 μm (*A*), 89.1 μm (*B*), 79.7 μm (*C*), 59.1 μm (*D*), 66.5 μm (*E*), and 73.2 μm (*F*).

Image Analysis. All image calculations were carried out in floating point format and images converted into eight-bit unsigned images for presentation using the imaging software WIT. The GP was calculated for each pixel using the two Laurdan intensity images ($I_{400-460}$ and $I_{470-530}$). GP images (as eight-bit unsigned
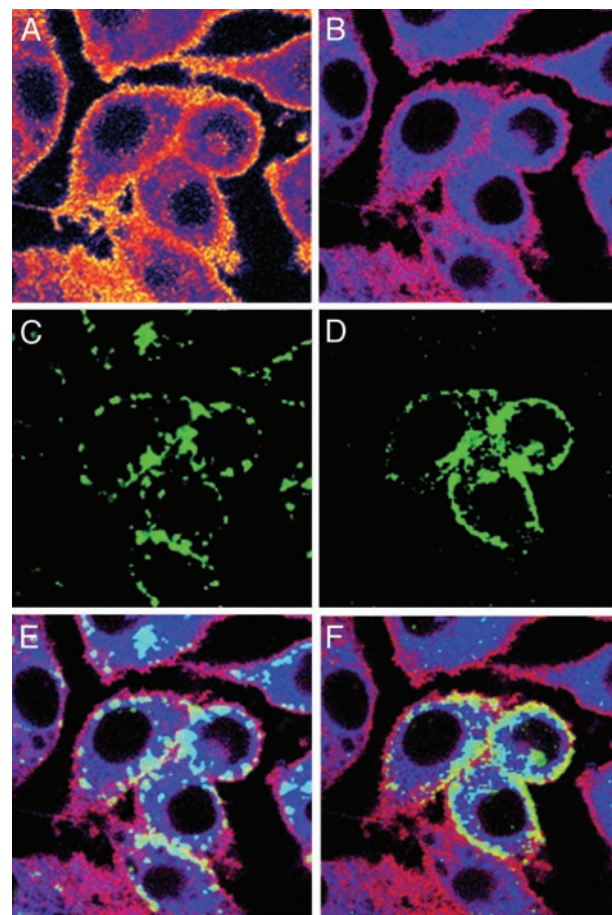

Fig. 3. Colocalization of caveolin-1 and transferrin receptor with high or low GP domains. A single GP image (*A*) was converted into a dual-colored image so that GP domains of GP <0.3 are blue, and domains with GP >0.3 are red (*B*). Single-photon confocal immunofluorescent images for transferrin receptor (*C*) and caveolin-1 (*D*) were obtained as outlined in *Methods*, pseudocolored green, and merged with *B* [transferrin receptor (*E*), caveolin-1 (*F*)]. Light blue indicates a colocalization with low GP domains, and yellow indicates a colocalization with high GP domains. The width of each image is 47.3 μm.

images) were pseudocolored in Adobe PHOTOSHOP (Adobe Systems, Mountain View, CA) and stacks of GP images (50–100 slices) reconstructed in VOXVIEW. Background values (defined as intensities below 7% of the maximum intensity) were set to zero and colored black. GP distributions were obtained from the histograms of the GP images (or stacks of images) and fitted to one or two Gauss distributions by using the nonlinear fitting algorithm (Microsoft EXCEL). GP values (e.g., center values)

Table 1. Two Gauss distributions of deconvoluted stacks of GP images

Cell type (condition)	Center 1	Width 1	Center 2	Width 2	Coverage 2, %
RAW (living)	0.18 (0.011)	0.29 (0.055)	0.52 (0.0059)	0.17 (0.038)	44.2 (6.9)
hMDM (living)	0.26 (0.011)	0.21 (0.095)	0.58 (0.076)	0.14 (0.042)	29.1 (6.1)
THP-1 (living)	0.11 (0.0086)	0.41 (0.028)	0.57 (0.028)	0.23 (0.046)	35.2 (10.4)
RAW (fixed)	0.17 (0.063)	0.22 (0.022)	0.42 (0.014)	0.25 (0.042)	32.6 (4.4)
RAW (mCD-Chol)	0.18 (0.031)	0.23 (0.031)	0.48 (0.010)	0.12 (0.064)	58.9 (7.5)
RAW (mCD)	0.11 (0.011)	0.32 (0.038)	0.39 (0.013)	0.15 (0.027)	37.3 (6.1)

Living RAW264.7, hMDM, and phorbol 12-myristate-differentiated THP-1 cells were imaged at 22°C (1.2×10^6 cells/3.14 cm^2). Living RAW264.7 cells were pretreated at 22°C with 1.0 mg/ml mCD for 10 min or 0.5 mg/ml cholesterol-complexed mCD (mCD-Chol) for 1 h. Where indicated, Laurdan-labeled (30 min, 0.5 μM) RAW264.7 cells were fixed in 4% paraformaldehyde at 4°C for 20 min. Stacks of GP images, as shown in Fig. 1, were fitted to two Gauss distributions, and the centers, widths, and percentage of pixels associated with center 2 (''coverage'') were averaged over 8–15 stacks.

Table 2. Deconvolution of single immunolabeled GP images at room temperature and characteristics of isolated lipid rafts

GP distribution (1-Gauss) of immunofluorescently masked images			
Primary antibody against	Center	Width	Pixels %
Caveolin-1	0.38 (0.026)	0.34 (0.085)	31.2 (11.5)
Flotillin-1	0.35 (0.019)	0.39 (0.064)	5.7 (2.2)
Caveolin-2	0.23 (0.016)	0.26 (0.17)	1.1 (0.96)
ABCA-1 + cAMP	0.23 (0.095)	0.44 (0.10)	19.3 (9.0)
ABCA-1	0.13 (0.0058)	0.29 (0.094)	10.7 (2.5)
Transferrin receptor	0.17 (0.014)	0.28 (0.059)	21.3 (8.3)
GP values of isolated membrane domains			
Isolation method	Sonication	0.2% Triton	0.2% Lubrol
RAW whole-cell fractionation (22°C)	0.477 ± 0.087	0.468 ± 0.103	0.418 ± 0.075
	(0.164 ± 0.054)	(0.206 ± 0.061)	(0.262 ± 0.094)
RAW PM fractionation (22°C)	0.493 ± 0.067	0.516 ± 0.062	0.339 ± 0.117
	(0.183 ± 0.036)	(0.229 ± 0.030)	(0.150 ± 0.081)
RAW PM fractionation (37°C)	0.359 ± 0.064	0.424 ± 0.048	0.308 ± 0.126
	(0.002 ± 0.070)	(0.071 ± 0.031)	(−0.071 ± 0.049)
Cellular cholesterol content associated with lipid rafts, %			
Isolation method	Sonication	0.2% Triton	0.2% Lubrol
RAW (untreated)	13.6 ± 2.7	47.5 ± 4.8	68.1 ± 2.2
RAW (mCD)	9.8 ± 2.1	41.6 ± 2.0	63.2 ± 3.4
	−31.5%	*−15.6%*	*−4.1%*
RAW (mCD-Chol)	17.3 ± 1.2	54.9 ± 2.7	67.5 ± 2.0
	+34.2%	*+17.5%*	*−1.9%*

At the top, immunofluorescent confocal images were used to mask the GP images of fixed RAW264.7 (see also Table 1), and the distribution of the resulting ''masked'' GP was fitted to a single Gauss distribution, and results were averaged over 6–12 images containing an average of three cells each. Where indicated, living RAW cells were treated with 0.3 mM cAMP for 30 min at 37°C prior to Laurdan labeling and fixing. At the middle and bottom, lipid raft and nonraft domains from RAW264.7 were isolated (see *Methods*). At the middle, isolated domains were labeled with Laurdan (0.05 mM, room temperature, 30 min) to determine the GP value at 22°C or 37°C. Values ± SD (*n* = 3) are given for lipid rafts; nonraft data are in parentheses. At the bottom, data show manipulation of lipid raft cholesterol content by treatment of RAW264.7 with mCD or cholesterol-complexed mCD (mCD-chol), as described in Table 1. Data are mean ± SD (*n* = 3). Changes in raft cholesterol relative to untreated cells are shown in italics.

were corrected by using G factor obtained for Laurdan in DMSO. G factor had <2% variation across the imaging area.

For comparison with GP images, confocal images were converted to binary images (with background value set to zero and above-background intensities set to one) and multiplied with the corresponding GP image. The histogram of these multiplied images was regarded as the GP distribution of the confocal images. GP values of confocal images could not be corrected, because the G factor for fixed cells in mounting fluid and residual paraformaldehyde could not be accurately determined.

Results and Discussion

Laurdan-stained macrophage images were collected at different focal depths and GP images calculated as described above. Fig. 1 shows pseudocolored GP images of RAW264.7 (mouse; Fig. 1*A*) and THP-1 (human; Fig. 1*B*) macrophages that have been reconstructed to a 3D image from 50–100 images. The GP images, as well as distribution of GP values (Fig. 1*C*), clearly show nonarbitrary differences in GP values across the cell surface. RAW264.7 macrophages exhibit knob-like membrane protrusions that colocalize with areas of high GP, indicating condensed, possibly raft-like domains. These membrane evagi-nations are also found on THP-1 macrophages but here, long slender filopodia are more common. These surface morphologies, cell-to-cell contacts, and possibly adhesion points (Fig. 1*B*) are also enriched with high GP domains. Primary hMDMs also display high GP filopodia but also have membrane invaginations that do not always colocalize with high GP domains (data not shown). Studies with liposomes have established that membranes with high curvature have lower GP values, i.e., appear more fluid than membrane areas with lesser curvature (15). Hence the high GP values we observe at filopodia, adhesion points, and cell–cell

contact points most likely reflect the condensed structure of the membrane, not altered curvature.

Areas enriched in high GP domains are from several hundred nanometers to micrometers in diameter. Lipid raft size estimates are controversial, with suggested sizes varying from 30 to 50 nm (12) to several micrometers (11); different techniques, cell types, and molecules tagged and tracked could account for the considerable differences. Two-photon fluorescence microscopy has limitation in spatial resolution (183 nm at 800 nm) and is not capable of visualizing individual rafts of previously predicted diameter. However, discrimination between high vs. low GP domains indicates either that individual small rafts cluster in certain membrane morphologies or that lipid raft size in macrophages has previously been underestimated. When living or fixed fibroblasts are imaged (Fig. 2 *A* and *B*), some, but relatively few, high GP domains at cell–cell contact points are seen. More high GP domains are revealed when fibroblasts are crosslinked nonspecifically (Fig. 2*D*) or patched with specific antibodies (Fig. 2*E*) as described (27, 28). Crosslinking of either raft or nonraft membrane proteins causes coalescence of common lipid microdomains, segregating larger areas of both raft and nonraft domains on the plasma membrane (28). Disruption of lipid rafts (10 mM mCD at 37°C for 1 h) causes complete loss of high GP domains (Fig. 2*C*), and remaining domains cannot be revealed by patching (Fig. 2*F*), as reported (31), but contrary to the findings by Hao *et al.* (32).

Studies of protein diffusion in and out of rafts suggest that these domains are highly dynamic, although some raft components have residence times of several minutes (12). Domains of high GP in macrophages were stable for at least 30 sec at room temperature, thereby allowing intensity images to be averaged. Surface area covered by lipid raft domains has been difficult to
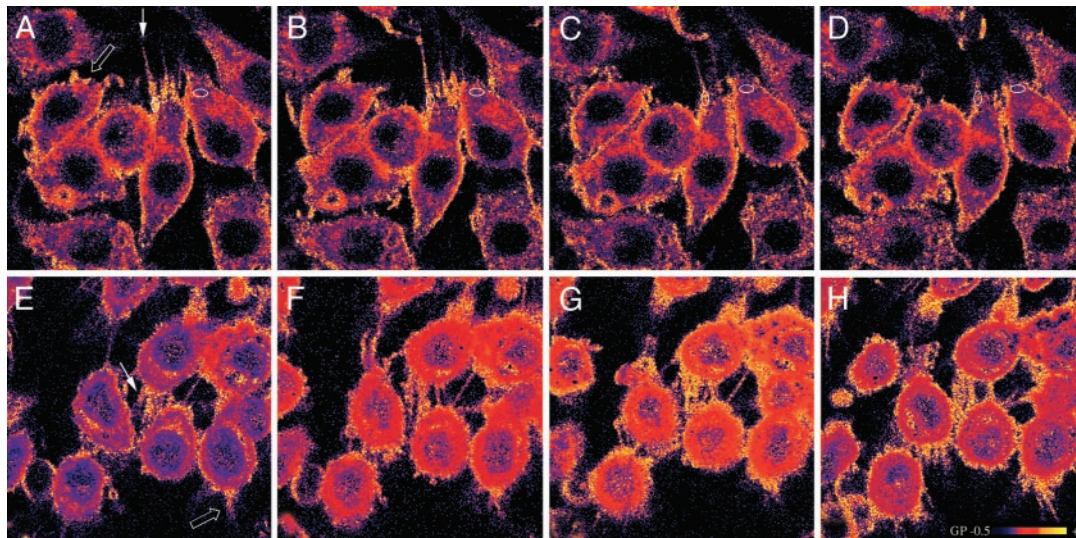
CELL BIOLOGY

Fig. 4. GP images of living cells with varied cholesterol content. RAW264.7 cells were treated at 22°C with mCD (1.0 mg/m) for 0 min (*A*), 2.5 min (*B*), 5 min (*C*), and 10 min (*D*), or with mCD-Chol (0.5 mg/ml) for 0 min (*E*), 5 min (*F*), 25 min (*G*), and 60 min (*H*). Images were pseudocolored, as indiciated in *H*. (*A–D*) Vertical and horizontal eclipses (each 260 pixels, 3.3 μm^2) indicate a high (mean GP = 0.57, decreasing by -0.044 min^{-1}) and low (mean GP = 0.081, decreasing by -0.0074 min^{-1}) GP domain, respectively. Filled arrow indicates a filopodium retracting during mCD treatment; open arrow, a membrane evagination appearing to pinch off. (*E–H*) The initial (0–25 min) shift to higher GP values on cholesterol loading declines after 60 min, although some filopodia remain more condensed. Open arrow indicates a membrane evagination extending during treatment; closed arrow shows increasing cell–cell contact points. Note an additional cell migrating from the left. Widths: 58.0 μm (*A–D*) and 51.2 μm (*E–H*).

determine, because the number of individual rafts per cell cannot be readily counted. Prior *et al.* (33), using immunogold electron microscopy, estimated that 35% of the cell surface is covered by rafts with a mean diameter of 44 nm. We deconvoluted the histograms of stacks of GP images to obtain two populations of high and low GP (Fig. 1*C*). The number of pixels associated with a given GP is an indication of the surface area of that population. The estimation of surface coverage is likely to be most accurate for macrophages, where domains of high GP values cluster to reach sizes above the resolution limit of the microscope (183 nm) in specific membrane morphologies. In other cells, such as fibroblasts, where clustering of visible lipid raft-rich regions may be less pronounced, deconvolution of the GP images may underestimate the surface area covered by lipid rafts. High GP populations in macrophages cover on average 29–44% of the cells' surface. Table 1 gives the mean values of the two GP populations, together with the widths (half width of half maximum) of their Gaussian distributions. The GP data clearly indicate a coexistence of liquid phases in macrophage membrane with separation at GP values of 0.3–0.4. A comparison with liposomes [1:1:1 dioleoylphosphatidylcholine/ cholesterol/sphingomyelin (17)] suggests a coexistence of liquid-disordered membranes (lower GP population) and liquid-ordered membranes (higher GP population), although phase separation in these liposomes is lower (at GP ≈ 0.3) than found here. GP values for phase separation in cells and liposomes are expected to differ for two main reasons. First, cellular membrane order is probably affected by membrane proteins, which are absent in model systems. Second, measurements in liposomes are conducted in thermodynamic equilibrium, whereas in cells, there is a constant turnover of lipids and proteins. In our experiments with living cells, there is some overlap between the two main GP distributions resulting from broader population widths (see also Fig. 1*B*). This is distinct from model membranes, where, at room temperature, domains and populations are well separated with population widths of 0.15–0.25. The temperature dependency of GP populations is well documented in model systems (13–15, 17). The overlap between populations could reflect raft heterogeneity, with rafts of different structure and fluidity obscuring

clear separation. Raft lipid heterogeneity has been proposed to explain the differential detergent insolubility of proteins (34, 35), but little is known of the lipid composition and structure of various raft populations. Further, the scatter in the data does not allow a deconvolution into more than two populations.

Mean values and surface coverage of high GP domains were also temperature-dependent (Fig. 1*D*). As expected, with increasing temperature, all membranes become more fluid. In fact, mean values of both populations decreased in parallel so that the fluidity difference between the two populations is maintained at physiological temperatures. Slopes of -0.0112/°C and -0.0132/°C were determined for the centers of low and high GP population, respectively, when fitted to a linear regression line (R^2 for linear fit, and sigmoidal fitting curves are very similar). These values agree very well with the temperature dependency of GP values in artificial membranes that mimic cellular membrane lipid composition (slopes -0.008/°C to -0.012/°C, data not shown) and with the GP values of isolated lipid rafts or nonraft domains (Table 2), validating the deconvolution of the living cells. Surface coverage of the high GP population decreased rapidly with increasing temperature, so that at 37°C, the coverage by lipid raft-like domains was 10–15%. This surprising finding may reflect a decrease in individual raft size, or in raft abundance, or that rafts disperse to smaller more mobile units below the time and spatial resolution of the two-photon microscope.

With a liquid-ordered structure, the question remains whether a high GP population comprises or is identical to "lipid rafts." Rafts are usually separated by extraction with either detergents or sonication and isolated by density gradient centrifugation. Some membrane proteins are characteristically associated with (caveolin-1, caveolin-2, flotillin-1) or excluded from (transferrin receptor) the buoyant rafts, although varying isolation methods, particularly detergents, generate rafts with various protein compositions (35). We evaluated the colocalization of some proteins with GP domains in paraformaldehyde-fixed/saponin-permeabilized cells. It should be noted that fixation/ permeabilization does alter lipid structure; it decreases the surface coverage of the high GP domains (Table 1). Schuck *et al.*

(36) have shown that treatment with saponin can decrease the buoyancy of raft protein similar to cyclodextrin treatment, suggesting that permeabilization may alter raft structure (36). We used single-photon confocal immunofluorescent images to mask the GP images of the fixed cells (visualized in Fig. 3) and deconvoluted the resulting GP population to a single Gaussian distribution (Table 2). The widths of these immunostained populations are broad due to the spatial limitation of the confocal microscopy (37). The GP populations of caveolin-1 and transferrin receptor most clearly segregate with the high and low GP domains of fixed RAW264.7 cells, respectively. ABCA-1, which is Triton-soluble but partially Lubrol-insoluble, has GP populations between the two means ($0.17 < GP < 0.42$), giving further evidence of raft heterogeneity (see also GP values of Lubrol-insoluble membranes in Table 2). Furthermore, GP values of isolated rafts are in good agreement with the mean values found microscopically (Table 1), thereby validating identification of rafts by microscopy.

Although the dependency of raft structure on cholesterol is frequently assumed, the effect of removing or adding cholesterol by agents such as cyclodextrins has not been directly determined in living cells. Here we assess the effect of mCD on raft cholesterol content (Table 2) and raft structure in living RAW 264.7 cells (Fig. 4). Even at low concentration (1.0 mg/ml), where only $9.5 \pm 1.2\%$ of total cell cholesterol is removed after 10 min at 22°C, the morphology of the macrophages changes rapidly. The cells lose their characteristic membrane protrusions, and surface coverage of the high GP population falls (from 44% to 37%), and its mean raft GP shifts to more fluid values (from 0.52 to 0.39, Table 1; a statistically significant shift in population

with $P < 0.05$). Small high GP areas (GP $\approx$ 0.5–0.6, area 3–5 μm^2, circled in Fig. 4A) decrease in GP [-0.036 (± 0.011) min^{-1}] more rapidly than low GP (GP = 0.08–0.13) areas [-0.0066 (± 0.009) min^{-1}], suggesting that lipid raft structure is altered more severely than nonraft domains. Conversely, increasing cell cholesterol with cholesterol-complexed mCD (0.5 mg/ml for 1 h, 1.3-fold increase in cell cholesterol) caused an increase in raft coverage but no alteration in mean GP values. Morphologically, short-term incubations with cholesterol-complexed mCD increased the number of high GP-enriched filopodia and cell–cell contact points.

These data demonstrate that raft coverage and membrane fluidity in living cells are cholesterol- and temperature-dependent, and that rafts appear to associate with specific cellular structures such as filopodia. Direct microscopic visualization is uniquely placed to determine cellular mechanisms that govern lipid raft structure and their physiological roles. GP values of living cells may not always directly correspond to those obtained in artificial membrane systems. However, comparisons of GP values within cells clearly establish fluidity differences within the plasma membrane, and comparisons before and after treatments allow an insight into raft maintenance. At this time, GP images cannot replace traditional microscopy or biochemical lipid raft characterization but can facilitate studies of lipid rafts on living cells.

1. Simons, K. & Toomre, D. (2000) *Nat. Rev. Mol. Cell. Biol.* **1,** 31–39.
2. Brown, D. A. & London, E. (1998) *Annu. Rev. Cell Dev. Biol.* **14,** 111–136.
3. Ikonen, E. (2001) *Curr. Opin. Cell Biol.* **13,** 470–477.
4. Simons, K. & Ikonen, E. (1997) *Nature* **387,** 569–572.
5. London, E. (2002) *Curr. Opin. Struct. Biol.* **12,** 480–486.
6. Brown, D. A. & London, E. (1998) *J. Membr. Biol.* **164,** 103–114.
7. Brown, D. A. & London, E. (2000) *J. Biol. Chem.* **275,** 17221–17224.
8. London, E., Brown, D. A. & Xu, X. (2000) *Methods Enzymol.* **312,** 272–290.
9. Varma, R. & Mayor, S. (1998) *Nature* **394,** 798–801.
10. Kenworthy, A. K., Petranova, N. & Edidin, M. (2000) *Mol. Biol. Cell* **11,** 1645–1655.
11. Schutz, G. J., Kada, G., Pastushenko, V. P. & Schindler, H. (2000) *EMBO J.* **19,** 892–901.
12. Pralle, A., Keller, P., Florin, E. L., Simons, K. & Horber, J. K. (2000) *J. Cell Biol.* **148,** 997–1008.
13. Bagatolli, L. A. & Gratton, E. (2000) *Biophys. J.* **78,** 290–305.
14. Bagatolli, L. A. & Gratton, E. (2000) *Biophys. J.* **79,** 434–447.
15. Bagatolli, L. A. & Gratton, E. (1999) *Biophys. J.* **77,** 2090–2101.
16. Bagatolli, L., Gratton, E., Khan, T. K. & Chong, P. L. (2000) *Biophys. J.* **79,** 416–425.
17. Dietrich, C., Bagatolli, L. A., Volovyk, Z. N., Thompson, N. L., Levi, M., Jacobson, K. & Gratton, E. (2001) *Biophys. J.* **80,** 1417–1428.
18. Dietrich, C., Volovyk, Z. N., Levi, M., Thompson, N. L. & Jacobson, K. (2001) *Proc. Natl. Acad. Sci. USA* **98,** 10642–10647.
19. Parasassi, T., Gratton, E., Yu, W. M., Wilson, P. & Levi, M. (1997) *Biophys. J.* **72,** 2413–2429.
20. Bagatolli, L. A., Sanchez, S. A., Hazlett, T. & Gratton, E. (2003) *Methods Enzymol.* **360,** 481–500.
21. Tricerri, M. A., Sanchez, S. A., Arnulphi, C., Durbin, D. M., Gratton, E. & Jonas, A. (2002) *J. Lipid Res.* **43,** 187–197.
22. Harris, F. M., Best, K. B. & Bell, J. D. (2002) *Biochim. Biophys. Acta* **1565,** 123–128.
23. Bagatolli, L. A., Parasassi, T., Fidelio, G. D. & Gratton, E. (1999) *Photochem. Photobiol.* **70,** 557–564.
24. Bagatolli, L. A., Parasassi, T. & Gratton, E. (2000) *Chem. Phys. Lipids* **105,** 135–147.
25. Gaus, K., Gooding, J. J., Dean, R. T., Kritharides, L. & Jessup, W. (2001) *Biochemistry* **40,** 9363–9373.
26. Peiser, L., Gough, P. J., Kodama, T. & Gordon, S. (2000) *Infect. Immun.* **68,** 1953–1963.
27. Friedrichson, T. & Kurzchalia, T. V. (1998) *Nature* **394,** 802–805.
28. Harder, T., Scheiffele, P., Verkade, P. & Simons, K. (1998) *J. Cell Biol.* **141,** 929–942.
29. Gaus, K., Dean, R. T., Kritharides, L. & Jessup, W. (2001) *Biochemistry* **40,** 13002–13014.
30. Roy, S., Luetterforst, R., Harding, A., Apolloni, A., Etheridge, M., Stang, E., Rolls, B., Hancock, J. F. & Parton, R. G. (1999) *Nat. Cell Biol.* **1,** 98–105.
31. Vainio, S., Heino, S., Mansson, J. E., Fredman, P., Kuismanen, E., Vaarala, O. & Ikonen, E. (2002) *EMBO Rep.* **3,** 95–100.
32. Hao, M., Mukherjee, S. & Maxfield, F. R. (2001) *Proc. Natl. Acad. Sci. USA* **98,** 13072–13077.
33. Prior, I. A., Muncke, C., Parton, R. G. & Hancock, J. F. (2003) *J. Cell Biol.* **160,** 165–170.
34. Madore, N., Smith, K. L., Graham, C. H., Jen, A., Brady, K., Hall, S. & Morris, R. (1999) *EMBO J.* **18,** 6917–6926.
35. Roper, K., Corbeil, D. & Huttner, W. B. (2000) *Nat. Cell Biol.* **2,** 582–592.
36. Schuck, S., Honsho, M., Ekroos, K., Shevchenko, A. & Simons, K. (2003) *Proc. Natl. Acad. Sci. USA* **100,** 5795–5800.
37. White, J. G., Squirrell, J. M. & Eliceiri, K. W. (2001) *Traffic* **2,** 775–780.

CELL BIOLOGY